This is a repository copy of *Transient viscoelastic lubrication analyses of UHMWPE hip replacements*.

White Rose Research Online URL for this paper:
http://eprints.whiterose.ac.uk/133835/

Version: Accepted Version

Transient viscoelastic lubrication analyses of UHMWPE hip replacements

Xianjiu Lu[a], Qingen Meng[b, *1], Jing Wang[c], Zhongmin Jin[a, b, d, *2]

[a] State Key Laboratory of Manufacturing System Engineering, School of Mechanical Engineering, Xi'an Jiaotong University, 99 Yanxiang Road, Xi'an, Shanxi, 710054, China

[b] School of Mechanical Engineering, University of Leeds, LS2 9JT, UK

[c] School of Mechanical Engineering, Qingdao University of Technology, Qingdao, China

[d] Tribology Research Institute, School of Mechanical Engineering, Southwest Jiaotong University, Chengdu, 610031, Sichuan, China

*1 Corresponding author:
Tel: 44 113 343 8893
Fax: 44 113 242 4611
Email: Q.Meng@leeds.ac.uk

*2 Corresponding author:
Tel: 0086-13689289660
Email: zmjin@mail.xjtu.edu.cn

Abstract

The viscoelasticity of the UHMWPE liner may play an important role in the lubrication performance of soft artificial hip joints. All the previous lubrication analyses for UHMWPE hip implants assumed that the UHMWPE liner was linear elastic. In order to investigate the influence of viscoelasticity of the UHMWPE liner, a transient viscoelastic lubrication model was developed. The results showed that the viscoelasticity played a significant role in the lubrication performance of UHMWPE hip implants. Moreover, the retardation time and the ratio of loss and storage modulus of the UHMWPE liner had important effects on the lubrication performance of hip implants. These findings provide new insights into the lubrication mechanisms of UHMWPE artificial hip joints.

Keywords: Transient viscoelastic lubrication; UHMWPE artificial hip replacements; Viscoelasticity; Bio-tribology

1 Introduction

Viscoelasticity widely exists in biological and engineering systems. For example, articular cartilage exhibits viscoelastic mechanical behavior due to its biphasic structure (consisting of a solid matrix phase and an interstitial fluid phase). Moreover, viscoelastic materials are also widely used in biomedical devices, such as the ultra high molecular weight polyethylene (UHMWPE) in low modulus artificial hip replacements. The deformation process of soft viscoelastic materials, such as polymers and elastomers, may display significant time lags and the viscoelastic effect may have to be considered in tribological analyses [1, 2]. However, due to the complexity of the tribological systems and the time-dependent properties of the materials, it is difficult to include the realistic mechanical behavior of the viscoelastic materials in a lubrication analysis, which intends to predict the pressure distribution and lubricant film thickness of a lubricated system.

The tribological performance of joint replacements determines the long-term service of these medical devices. Proper lubrication analysis can not only assess the lubrication regime but also assist in determining design and manufacturing parameters. One of the most popular artificial hip designs utilizes a material combination of a UHMWPE liner against a metal or ceramic femoral head. Early lubrication analyses 1 of such hip implants were conducted using a so-called constrained column method, in which the deformation at a given point of the UHMWPE liner was only linearly related to the local pressure applied to that point. The reason for employing the simple constrained column model was mainly because there were no full-field analytical solutions for the mechanical deformation of the ball-in-socket geometry. This limitation was overcome by Jagatia and Jin [3, 4] using the finite element method (FEM) to calculate the elastic influence coefficients. However, the calculation process was complex and time consuming. Wang and Jin [5] developed a method in which the elastic influence coefficients were fitted based on the normal displacements at the nodes along a longitudinal line and the elastic deformation was calculated using a spherical fast Fourier transform (SFFT) technique [5]. The SFFT technique improved the calculation efficiency significantly and has been incorporated in the lubrication

analyses of artificial hip joints [6, 7]. The deformation of the bearing surfaces in all the above lubrication analyses were assumed to be linear elastic, which is reasonable for hard-on-hard materials. However, if the viscoelasticity of UHMWPE needs to be considered, the above methodology may be no longer valid.

Indeed, the viscoelasticity of bearing materials can have significant influences on the lubrication performance. For instance, although Rohde et al [8] found that the viscoelasticity effects was minor for a squeeze film lubrication model, both Yoo et al [9] and Kaneko et al [10] found that when the viscoelastic effect was considered in the squeeze film model, the solutions were remarkably different from those of the elastohydrodynamic lubrication (EHL). Moreover, through solving the line contact lubrication problem, Elsharkawy [11], Hooke et al [12], Scaraggi et al [13] and Pandey et al [14] all found that the viscoelastic effects of the bearing materials may considerably affect the lubrication performance of the system. Furthermore, using a point contact lubrication model, Putignano et al [15] confirmed that if the viscoelasticity of the bearing surfaces was considered, the pressure distributions, film thickness and friction of a lubrication system were significant different from the classical EHL regime response. However, the viscoelastic effects of the UHMWPE liner on the lubrication performance of soft artificial hip joints remain unclear due to the lack of an effective numerical process.

Therefore, the aim of the present study was to investigate the effects of the viscoelasticity of the UHMWPE liner on lubrication performance of the UHMWPE artificial hip joints using a new numerical procedure, which can simulate the lubrication performance of viscoelastic materials under arbitrary loading histories and contact profiles.

2 Materials and methods

2.1 Materials

A standard 28 mm diameter hard material on polyethylene hip implant, which consists of a metal or ceramic femoral head and a UHMWPE liner, was analyzed. The radius of the cup and head was 14.05 and 14 mm, respectively. The thickness of the

UHMWPE liner was 9.5 mm. The instantaneous elastic modulus and Poisson's ratio of UHMWPE was 700 MPa and 0.4, respectively. Since this was the first attempt to investigate the viscoelastic effects of the UHMWPE liner on the lubrication performance of soft artificial hip joints, a relatively large viscosity (0.01 Pa s) was adopted for the lubricant. The material and geometrical parameters were summarized in Table 1.

2.2 Theory of viscoelasticity

According to the creep response process of viscoelastic materials, the responses of strain exhibit highly time-dependent characteristics. In order to characterize the viscoelastic properties of such a material, the strain response function was defined as [16, 17]:

$$\varepsilon(t) = \sigma_0 J(t) \tag{1}$$

where J(t) is the creep compliance function representing the time-dependent strain (ε(t)) under a unit constant stress (σ_0).

With regard to the creep response characteristics, the creep compliance of the standard linear viscoelastic model was

$$J(t) = \frac{1}{E_2}\left[1 + \frac{E_2}{E_1}(1 - e^{-\frac{t}{\tau}})\right] \tag{2}$$

where E_2 represents the storage modulus (instantaneous elastic modulus), E_1 the loss modulus , and τ the retardation time defined as η_u/E_1 (where η_u is viscosity of the viscoelastic material), which can be estimated by the time required after release of stress for the strain to decrease to 1/e (0.368) of its original value[18].

The above viscoelastic model was considered as the combination of two springs and a dashpot (Fig 1). The response of a viscoelastic material to an arbitrary stress profile was obtained by decomposing the loading history into a series of small steps. Therefore, the strain resulted from these small steps was superposed to obtain the final strain at time t by the Boltzmann hereditary integral [16, 17]:

$$\varepsilon(t) = \int_0^t J(t - \xi)\frac{d\sigma(\xi)}{d\xi}\,d\xi \tag{3}$$

2.3 Lubrication model

A ball-in-socket model was used to represent the articulation of the cup and head (Fig

2). The cup was assumed to be positioned horizontally under the vertical load w_y. Only the flexion/extension angular velocities ω_z were considered as they play a dominant role during the daily working of hip joints. A Leeds Prosim hip simulator walking pattern (Fig 3) was considered in this study.

The time-dependent Reynolds equation in spherical coordinates used in this study was [19]

$$\sin\theta \frac{\partial}{\partial\theta}\left(\frac{h^3}{\eta}\sin\theta \frac{\partial p}{\partial\theta}\right) + \frac{\partial}{\partial\phi}\left(\frac{h^3}{\eta}\frac{\partial p}{\partial\phi}\right) = 6R_c^2 \sin^2\theta\left[\omega_z \frac{\partial h}{\partial\phi} + 2\frac{\partial h}{\partial t}\right] \tag{4}$$

where p is the hydrodynamic pressure; h is the thickness of the lubricant film; R_c is the radius of the head; t is time; η is the viscosity of the periprosthetic synovial fluid; ω_z is the angular velocity of the femoral head; and ϕ and θ are the spherical coordinates defined in Fig 2.

The external load components imposed on the acetabular cup was balanced by the resultant forces on the cup generated by the film pressure:

$$f_x = R_c^2 \int_0^\pi \int_0^\pi p \sin^2\theta \cos\varphi d\theta d\varphi = 0 \tag{5}$$

$$f_y = R_c^2 \int_0^\pi \int_0^\pi p \sin^2\theta \sin\varphi d\theta d\varphi = w_y(t) \tag{6}$$

$$f_z = R_c^2 \int_0^\pi \int_0^\pi p \sin\theta \cos\theta d\theta d\varphi = 0 \tag{7}$$

where R_c is the radius of the cup and W_y is the loading applied. Since only the vertical and flexion/extension motions were considered in the present analysis, the load ad balance equation along z direction was satisfied automatically.

The film thickness consisted of the undeformed gap of the spherical bearing surfaces and the viscoelastic deformation due to the present and history hydrodynamic pressures:

$$h(\varphi, \theta, t) = c - e_x \sin\theta \cos\varphi - e_y \sin\theta \sin\varphi + \delta(\varphi, \theta, t) \tag{8}$$

where δ is the viscoelastic deformation of the UHMWPE cup; c is the radial clearance between the cup and the head; and e_x and e_y are eccentricities of the femoral head.

2.4 Numerical methods

2.4.1 Algorithm description

6

In order to facilitate the numerical process and improve the stability, the governing equations were non-dimensionalized. A multi-grid method [20, 21] was used to solve the Reynolds equation. On each grid level, the finite difference method was used to approximate the Reynolds equation. The central difference was applied to the left hand side of the equation and the backward difference to the right hand terms. The detailed numerical approach was similar to that of the linear elastic model in the previous publications [20, 21].

To consider the memory effect of viscoelastic materials, the time domain was discretized into 128 small time steps, which were identical to the employed instants of a walking cycle. The pressure distributions were assumed unchanged in each time step. The pressure at node (k, l) after γ time increments was denoted by $p_{k, l, \gamma}$, therefore, the pressure increment in the γth time step was $p_{k, l, \gamma} - p_{k, l, \gamma-1}$. Based on the Boltzmann hereditary integral, the displacement considering the viscoelastic effect at node (i, j) after γ time steps was written as:

$$\delta^k_{i,j,\gamma} = \sum_{\gamma'=1}^{\gamma} \sum_{k=0}^{n^k_\phi} \sum_{l=0}^{n^k_\theta} K^{vs}_{i-k,j-l,\gamma-\gamma'} \left(p^k_{k,l,\gamma} - p^k_{k,l,\gamma-1} \right) \tag{9}$$

where, $K^{vs}_{i-k,j-l,\gamma-\gamma'}$ is the viscoelastic coefficient, representing the viscoelastic deformations after γ time steps in the element (i, j) caused by a unit pressure acted on the element (k, l) in all the previous γ' time steps ($\gamma' \leq \gamma$).

The viscoelastic deformation coefficients were derived by the creep compliance function and linear elastic coefficients as follows:

$$K^{vs}_{i-k,j-l,\gamma} = J(\gamma) D_{i-k,j-l} \tag{10}$$

where, $D_{i-k,j-l}$ is the deformation coefficients of the model when only the instantaneous elastic modulus E_2 and Poisson's ratio υ were considered.

Equation (9) shows that all pressure distributions in the previous γ-1 time steps were needed to calculate the viscoelastic deformation at time t = $\gamma\Delta$t. Therefore, once the pressure at γ' ($\gamma' \leq \gamma$) time instant was obtained, it was saved for the calculation of the viscoelastic deformation at the γth time step. As the multi-grid method was employed to calculate the discretized Reynolds equation, the viscoelastic deformation

calculation was implemented more than once during each W cycle. Hence, the most time consuming step of the transient viscoelastic lubrication analysis was the calculation of the viscoelastic deformation caused by the hydrodynamic pressure history. Since the viscoelastic deformation (Equation (9)) is a discrete convolution between viscoelastic deformation coefficients and hydrodynamic pressure increment of the γth time step, the deformation was calculated using the 2-based decimation-in-frequency fast Fourier transform (FFT) algorithm [5, 22, 23], in order to improve the calculation efficiency (reducing the time complexity from $O\left(N_1^2 N_2^2\right)$ to $O\left(N_1 N_2 \log_2\left(N_1 N_2\right)\right)$.

2.4.2 Calculation of the instantaneous elastic and viscoelastic deformation coefficients

The instantaneous elastic deformation coefficients of the cup surface ($D_{i-k,j-l}$) were calculated using a finite-element-based method (Wang and Jin 2004). A unit pressure was applied to an element located at the center of the inner surface of the cup. The displacement distribution along a longitudinal line caused by the unit pressure was calculated in ABAQUS 6.14 (Dassault Systèmes Simulia Corp, United States). These displacement coefficients were subsequently used to curve fit a displacement influence function making use of the spherical distance as the independent variable. The deformation coefficients of all other nodes on the surface were calculated based on this function. Because three levels of grid were adopted for the MG method, the influence coefficients of different meshes (65×65，129×129，and 257×257 nodes) were calculated and saved for the use in the numerical analysis. Based on the instantaneous elastic coefficients and creep compliance function, the viscoelastic coefficients were obtained for each time instant over a gait cycle using equation (10).

The accuracy of the elastic and viscoelastic deformation coefficients were checked by calculating the deformation caused by a given pressure distribution and then comparing with the deformation obtained from a finite element analysis (FEA). In order to achieve this, a parabolic pressure distribution with the maximum pressure of 10 MPa and a half contact angle of 30 degrees was applied to the bearing surface of the cup. When the elastic deformation coefficients were verified, the cup was assumed

to be elastic, and the deformation calculated by the elastic deformation coefficients was compared with that by the FEA. When the viscoelastic deformation coefficients were verified, the cup was viscoelastic and the pressure distribution was held for a period of time (i.e. 40 s). Then the viscoelastic deformation was calculated at several time instants (1s, 10 s, 20 s, 40 s) using both the FEM and present numerical method and compared.

To verify the numerical method further, the variation of the viscoelastic coefficient of a node with time under the action of a unit constant pressure was also calculated using Equation (10). In order to provide more verification, the effect of different retardation times (from 4 s to 100 s) on the viscoelastic coefficient of a node was also investigated.

2.5 Comparison scheme

In order to investigate the effects of the viscoelasticity of the UHMWPE, the maximum pressure, minimum film thickness, deformation caused by the hydrodynamic pressure and the cross-sectional pressure and film thickness profiles along the entrainment direction were compared between the viscoelastic model and an elastic model. In the elastic model, the UHMWPE liner was assumed to be linear elastic with the modulus of 700 MPa.

In order to understand the effects of the retardation time (τ) and mechanical loss factor (the ratio of loss and storage modulus, E_1/E_2), a wide range of variations (4 s to 100 s for τ and 0.1 to 0.25 for E_1/E_2), which were all within a previous experimental test [2], were investigated. When the effect of the retardation time was investigated, mechanical loss factor was kept as a constant (0.14). When the effect of mechanical loss factor was investigated, the retardation time was a constant (13.81 s). Values of 0.14 and 13.81 s were chosen because they correspond to the normal body temperature (37°C) [2].

3 Results

The instantaneous elastic displacement influence coefficients and viscoelastic deformation coefficients of the UHMWPE cup employed in the present study were

both accurate enough (Figs 4 and 5). The deformations of the UHMWPE cup calculated from the deformation coefficients were all very close to those from the FEA (Figs 4 and 5). The biggest differences in the predicted maximum deformation between the deformation coefficients and the FEA were all below 1.2%.

The variation in the viscoelastic deformation coefficient of the node where a unit constant pressure was applied was shown in Fig 6. With the increase in time, the viscoelastic deformation coefficient increased until it reached to the equilibrium value, which was equal to the instantaneous elastic deformation. Moreover, with the increase of the retardation time, the time needed to reach the equilibrium value was longer.

The effects of the viscoelasticity of the UHMWPE liner on the lubrication performance were investigated by comparing the deformation, maximum pressure and minimum film thickness in a walking cycle between the elastic model and the viscoelastic model with the retardation time of 13.81s and loss factor 0.14 (Figs 7 and 8). The comparisons of the deformation and maximum pressure in a walking cycle between the elastic and viscoelastic models indicated that the viscoelasticity of the UHMWPE liner had a remarkable effect on the lubrication performance (Figs 7 and 8). The viscoelastic deformation at the center of the contact at the first and second load peaks were 64.8 and 72.2 μm, respectively (Fig 7). Compared with the linear elastic case, these values increased 3.6% and 14.7%, respectively. The maximum pressure in the elastic model at the two loading peaks during the walking cycle was both around 9.7 MPa. In the model considering the viscoelastic property, the maximum pressure at the first and second loading peaks was about 9.5 and 9.2 MPa, respectively. Moreover, in the viscoelastic model, the maximum pressure at 1.0 s was obviously lower than the value at 0.14 s, with a reduction of 14.5%. However, in the elastic model, the values at these two instants were almost the same since the loading at these instants was the same (300N). It is also worth noting that the effect of the viscoelasticity of the UHMWPE liner on the minimum film thickness was not considerable (Fig 8). The two curves were quite similar between 0-0.55 s. Compared with the elastic model, the film thickness of the viscoelastic model dropped a little before increased again and slightly overpassed that of the elastic model.

The effects of the viscoelasticity of the UHMWPE liner on the lubrication performance of hip implants were confirmed by the comparison of the cross-sectional pressure and film thickness profiles along the entrainment direction between the elastic model and the viscoelastic model (Fig 9). For instance, the maximum pressure at instant 1.0 s was much smaller than that of instant 0.14 s while the contact area at instant 1.0 s was larger than that of instant 0.14 s (Fig 9a). Moreover, the cross sectional pressure of the elastic model along the entrainment direction displayed very similar distributions at time instants 0.25 s and 0.65 s when the loading was similar. However, the pressure distributions of the viscoelastic model showed larger contact areas and much smaller maximum pressure (Fig 9a). At all the time instants presented in Fig 9b, the cross-sectional film thickness distributions of the viscoelastic model along the entrainment direction were slightly thicker than those of the elastic model.

With the decrease in the relaxation time of the UHMWPE liner, the hydrodynamic pressure decreased and the minimum film thickness became thicker (Figs 10 and 11). It is interesting to notice that with the increase in the relaxation time, the maximum pressure and film thickness of the viscoelastic model approached to those of the elastic model. When the relaxation time was 100 s, the difference became very small between the solutions of the viscoelastic model and the elastic model (Figs 10 and 11).

With the decrease in the ratio of loss and storage modulus (E_1/E_2) from 0.25 to 0.1, the maximum pressure decreased and the difference became more apparent in the stand phase during which the loading was heavier (Figs 12 and 13). It should be noted that when the ratio increased from 0.1 to 0.25, the maximum pressure and minimum film thickness tended to approach to those of the elastic model (Fig 12). Moreover, as shown in the pressure distribution and film thickness profiles (Fig 13), the contact area became larger and the pressure decreased as E_1/E_2 decreased. The general film thickness distribution indicated an increasing trend as E_1/E_2 decreased although the minimum film thickness decreased at time instant 0.65 s.

4 Discussion

In all the previous studies [3, 24-29] that investigated the time-dependent lubrication performance of UHMWPE hip replacements, only the Reynolds equation considered the effects of the previous time instant on the present instant. The deformation at a given instant was determined by the hydrodynamic pressure of that single instant. However, the deformation of the viscoelastic materials is a different scenario. Due to the time-dependent properties of the materials, the viscoelastic deformation depends on not only the present pressure distributions but also the loading history. A new model and numerical procedure have to be developed to consider the viscoelastic deformation in UHMWPE artificial hip joints. As a result, the viscoelastic effects of the UHMWPE liner on the lubrication performance of artificial hip joints are still not clear. Therefore, the aim of this study was to investigate the effects of the viscoelasticity of the UHMWPE liner on the lubrication performance of artificial hip joints with an effective numerical process.

The validity of the numerical method developed in this study was supported by the following facts. First, the deformation calculated by the numerical method developed in this study agreed very well with that by the FEA (Fig 5), which indicated that the viscoelastic deformation coefficients used in this study were reliable. Secondly, with the increase of time, the viscoelastic deformation at a node under unit pressure calculated using Equation (10) approached to the equilibrium deformation of the material (Figure 6), which provided more validation for the viscoelastic deformation coefficients used in the numerical analyses. In addition, the results of the lubrication analyses were physically reasonable. For instance, it is reasonable to consider the elastic lubrication model as a special case of the viscoelastic lubrication model when the value of the relaxation time is large enough. This is because the viscoelastic time lag response will be so long that the residual deformation of the previous time instants can hardly have an obvious impact on the deformation at present time step. When the ratio of loss and storage modulus is large enough, the storage modulus plays a major role and the viscoelastic model should perform as the linear elastic case. The results produced in this study agreed with the above two arguments very well (Figs 10 and 12).

The inclusion of the viscoelastic effects did have considerable influences on the predicted lubrication performance of UHMWPE artificial hip joints. For instance, the predicted maximum pressure was smaller than that of the elastic model, and differences in the maximum pressure between the elastic model and viscoelastic model became more obvious with the increase of time (Fig 8). This was due to the influence of residual deformations at the previous time instants, which can be clearly seen from the variation of viscoelastic deformation during a gait cycle (Fig 7). In the viscoelastic model, the calculations of deformation of later time steps were based on the deformed geometry rather than the initial geometry. Therefore, the accumulated deformation was larger than that of the elastic model, which caused a larger contact area (Fig 9). As a result, the hydrodynamic pressure of the viscoelastic model was lower than that of the elastic model under the same applied load patterns. However, different from the monotonous decrease of the maximum hydrodynamic pressure, the film thickness displayed slight fluctuations compared with the elastic case (Fig 8). In other words, the viscoelasticity of the UHMWPE liner had little influence on the lubricating film thickness. This conclusion is consistent with a previous study [8].

It should be noted that the effect of the viscoelasticity on the pressure distribution seemed not the same as some previous studies. In the previous studies [12, 30], the pressure distribution was asymmetric when the viscoelasticity was considered. However, the pressure and film thickness distribution profiles of the viscoelastic lubrication model in this study resembled those of the pure elastic model. This may be because in the previous studies a pure rolling condition was considered. However, the relative motion in the artificial hip joints is pure sliding and the contact area of a fixed UHMWPE cup is the same as the pure squeeze film lubrication throughout the walking cycle, which is different from the pure rolling case.

The parametric analyses of this study may have important implications for the design of UHMWPE hip implants. For instance, this study found that with the decrease in the retardation time, the contact area and file thickness increase and the maximum pressure reduces (Figs 10 and 11). Moreover, with the decrease in the loss modulus, the influence of dashpot of the UHMWPE became more apparent and the viscoelastic

deformation was more likely to contribute to the lubrication performance of the hip implants (Figs 12 and 13). These findings may provide guidance for the future design of UHMWPE hip implants.

There are a few limitations in this study. First, it has been well known that the film thickness developed in UHMWPE hip joint was not large enough to separate the matting surfaces [6, 31]. In other words, the UHMWPE artificial hip joint usually works in a mixed lubrication environment. However, the surface profile of the UHMWPE liner was assumed to be smooth in this study. Secondly, in order to achieve a good convergence for the model and investigate the influence of viscoelasticity of UHMWPE liner on the transient lubrication performance of artificial hip joints, the viscosity used for the lubricant was larger than the realistic value. In addition, the accuracy of the proposed viscoelastic model was only verified for the case that the contact area is away from the edge of the cup. However, the edge loading conditions exist in reality. To account for such adverse conditions in the lubrication analyses, a more complex lubrication model considering the inclination of the cup and even lubricant starvation needs to be developed [32]. Furthermore, only one normal walking gait was considered in this study. However, the reciprocating motion of the joint may have important effects on the viscoelastic performance of UHMWPE. Therefore, it is necessary to investigate the oscillation through simulating more gaits and different types of motions such as slow walking, brisk walking, jogging and running. All these limitations will be addressed in future studies. Despite these limitations, this study has developed an effective model to study the effects of the viscoelasticity of UHMWPE liners on the lubrication performance of hip implants and showed that the viscoelasticity of the UHMWPE liner may play a significant role in the lubrication performance of hip implants.

5 Conclusions

A transient viscoelastic lubrication model was developed and solved in order to investigate the influence of viscoelasticity on the lubrication performance of UHMWPE artificial hip joints. The results showed that the viscoelasticity of bearing

surfaces played significant role in the lubrication performance and should not be ignored. Moreover, the relaxation time and the ratio of storage and loss modulus of the UHMWPE liner had important effects on the lubrication performance of the hip implants.

Conflicts of interest statement

There is no conflict of interest.

Acknowledgements

References

[1] Kwon-Yong L, David P. Compressive creep characteristics of extruded ultralhigh-molecular-weight polyethylene. Journal of biomedical materials research. 1997;39:261-5.

[2] Deng M, Uhrich K. Viscoelastic behaviors of ultrahigh molecular weight polyethylene under three-point bending and indentation loading. Journal of biomaterials applications. 2010;24:713-32.

[3] Jagatia M, Jalali-Vahid D, Jin ZM. Elastohydrodynamic lubrication analysis of ultra-high molecular weight polyethylene hip joint replacements under squeeze-film motion. Proceedings of the Institution of Mechanical Engineers Part H, Journal of engineering in medicine. 2001;215:141-52.

[4] Jagatia M, Jin ZM. Elastohydrodynamic lubrication analysis of metal-on-metal hip prostheses under steady state entraining motion. Proceedings of the Institution of Mechanical Engineers Part H, Journal of engineering in medicine. 2001;215:531-41.

[5] Wang FC, Jin ZM. Prediction of elastic deformation of acetabular cups and femoral heads for lubrication analysis of artificial hip joints. Proceedings of the Institution of Mechanical Engineers, Part J: Journal of Engineering Tribology. 2004;218:201-9.

[6] Wang FC, Jin ZM. Elastohydrodynamic Lubrication Modeling of Artificial Hip Joints Under Steady-State Conditions. Journal of Tribology. 2005;127:729.

[7] Wang FC, Jin ZM. Lubrication modelling of artificial hip joints. Springer Netherlands. 2006:385-96.

[8] Rohde S, Whicker D, Booker J. Elastohydrodynamic squeeze films: effects of viscoelasticity and fluctuating load. Journal of Lubrication Technology. 1979;101:74-80.

[9] Yoo H. Some Effects of Viscoelastic Matrix on the Squeeze Films. A S L E Transactions. 1987;30:403-8.

[10] Kaneko S, Tanaka T. A Study on Squeeze Films Between Porous Rubber Surface

and Rigid Surface: Analysis Based on the Viscoelastic Continuum Model. Journal of Tribology. 2004;126:719.

[11] Elsharkawy AA. Visco-elastohydrodynamic lubrication of line contacts. wear. 1996;199:45-53.

[12] Hooke C, Huang P. Elastohydrodynamic lubrication of soft viscoelastic materials in line contact. Proceedings of the Institution of Mechanical Engineers, Part J: Journal of Engineering Tribology. 1997;211:185-94.

[13] Scaraggi M, Persson B. Theory of viscoelastic lubrication. Tribology International. 2014;72:118-30.

[14] Pandey A, Karpitschka S, Venner C, et al. Lubrication of soft viscoelastic solids. Journal of Fluid Mechanics. 2016;799:433-47.

[15] Putignano C, Dini D. Soft Matter Lubrication: Does Solid Viscoelasticity Matter? ACS applied materials & interfaces. 2017;9:42287-95.

[16] Chen WW, Wang JQ, Huan Z, et al. Semi-Analytical Viscoelastic Contact Modeling of Polymer-Based Materials. Journal of Tribology. 2011;133:041404.

[17] Brinson H, Brinson L. Polymer engineering science and viscoelasticity: An Introduction. Springer, New York. 2008.

[18] Gooch JW. Retardation Time. In: Gooch JW, editor. Encyclopedic Dictionary of Polymers. New York, NY: Springer New York; 2011. p. 627-.

[19] Meng QE, Liu F, Fisher J, et al. Contact mechanics and lubrication analyses of ceramic-on-metal total hip replacements. Tribology International. 2013;63:51-60.

[20] Meng QE, Gao LM, Liu F, et al. Transient elastohydrodynamic lubrication analysis of a novel metal-on-metal hip prosthesis with an asspherical acetabular bearing surface. Journal of medical biomechanics. 2009;24:352-62.

[21] Gao LM, Meng QE, Wang FC, et al. Comparison of numerical methods for elastohydrodynamic lubrication analysis of metal-on-metal hip implants: multi-grid verses Newton-Raphson. Proceedings of the Institution of Mechanical Engineers, Part J: Journal of Engineering Tribology. 2007;221:133-40.

[22] Liu SB, Wang Q, Liu G. A versatile method of discrete convolution and FFT (DC-FFT) for contact analyses. Wear. 2000;243:101-11.

[23] Cooley JW, Tukey JW. An Algorithm for the Machine Calculation of Complex Fourier Series. Mathematics of computation. 1965;19:297-301.

[24] Jalali-Vahid D, Jagatia M, Jin ZM, Dowson D. Elastohydrodynamic lubrication analysis of UHMWPE hip joint replacements. Tribology Series. 2000;38:329-39.

[25] Jalali-Vahid D, Jagatia M, Jin ZM, & Dowson D. Prediction of lubricating film thickness in UHMWPE hip joint replacement. Journal of biomechanics. 2001;34:261-6.

[26] Jalali-Vahid D, Jin ZM. Transient elastohydrodynamic lubrication analysis of ultra-high molecular weight polyethylene hip joint replacement. Proceedings of the Institution of Mechanical Engineers, Part C: Journal of Mechanical Engineering Science. 2001;216:409-20.

[27] Jalali-Vahid D, Jagatia M, Jin ZM, et al. Prediction of lubricating film thickness in UHMWPE hip joint replacements. Journal of biomechanics. 2001;34:261-6.

[28] Jalali-Vahid D, Jin ZM, Dowson D. Elastohydrodynamic lubrication analysis of

hip implants with ultra high molecular weight polyethylene cups under transient conditions. Proceedings of the Institution of Mechanical Engineers, Part C: Journal of Mechanical Engineering Science. 2003;217:767-77.

[29] Mattei L, Di Puccio F, Piccigallo B, et al. Lubrication and wear modelling of artificial hip joints: A review. Tribology International. 2011;44:532-49.

[30] Abdallah AA. Visco-elastohydrodynamic lubrication of line contacts. wear. 1996;199:45-53.

[31] Jin ZM, Dowson D, Fisher J. Analysis of fluid film lubrication in artificial hip joint replacements with surfaces of high elastic modulus. Proceedings of the Institution of Mechanical Engineers, Part H: Journal of Engineering in Medicine. 1997;211:247-56.

[32] Meng QE, Wang J, Yang PR, et al. The lubrication performance of the ceramic-on-ceramic hip implant under starved conditions. Journal of the mechanical behavior of biomedical materials. 2015;50:70-6.

Table 1 Material and geometrical parameters adopted in the simulation

Radius of femoral head, R_H	14 mm
Radial clearance, c	50 μm
Thickness of UHMWPE cup	9.5 mm
Instantaneous elastic modulus of UHMWPE	700 MPa
Poisson's ratio of UHMWPE	0.4
Viscosity of 25% bovine serum solution	0.01 Pa.s
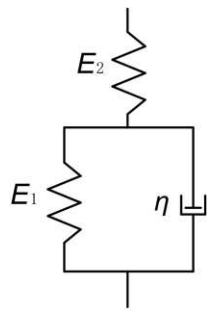
Fig. 1 The standard linear viscoelastic model adopted in this study
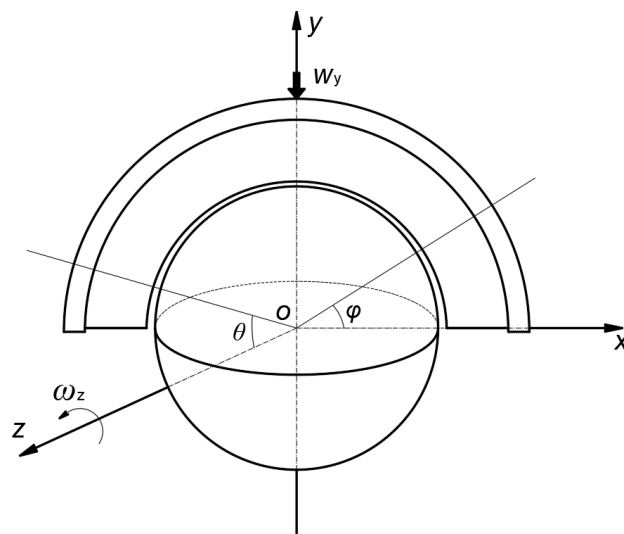
Fig. 2 The ball-in-socket lubrication model of the hip joint
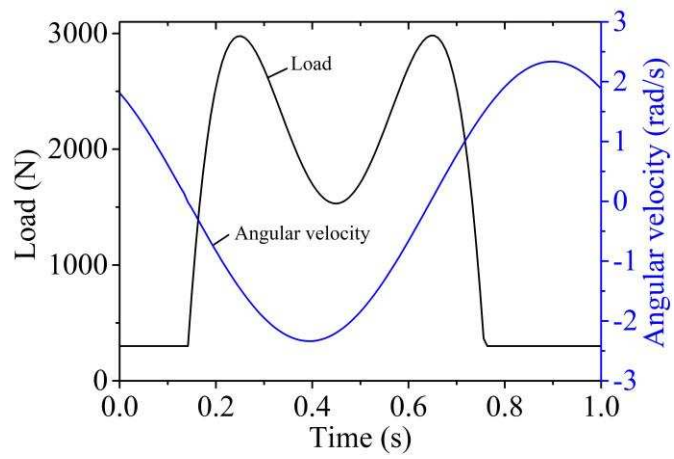
Fig. 3 Load and angular velocity profiles of Prosim hip simulator gait pattern
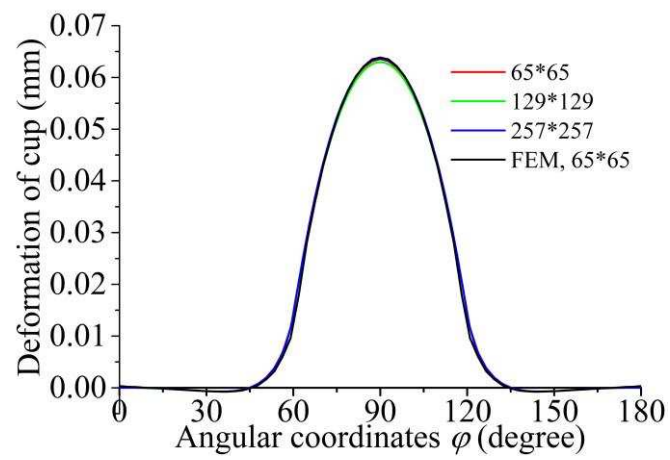
Fig. 4 The cross-sectional elastic deformation of the UHMWPE cup in the latitude direction under a parabolic pressure distribution with the maximum pressure of 10 MPa
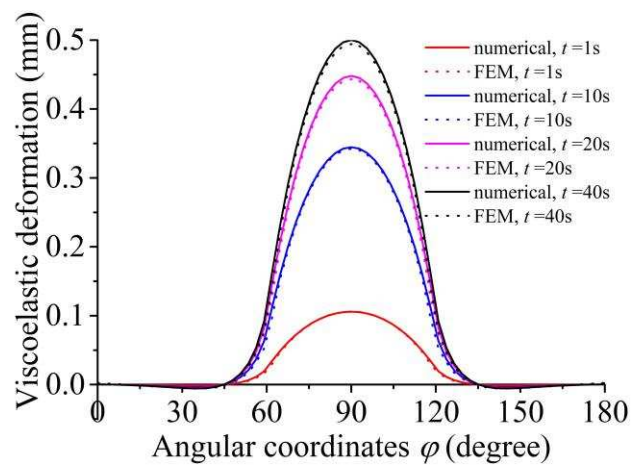
Fig. 5 The cross-sectional viscoelastic deformation of the UHMWPE cup in the latitude direction under a parabolic pressure distribution with the maximum pressure of 10 MPa ($\tau =10$s)
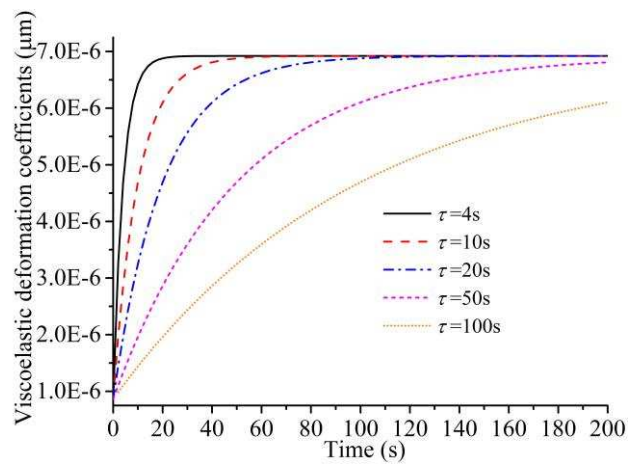
Fig. 6 The variation in the viscoelastic deformation coefficient of a node at the center of the cup under a unit constant pressure distribution
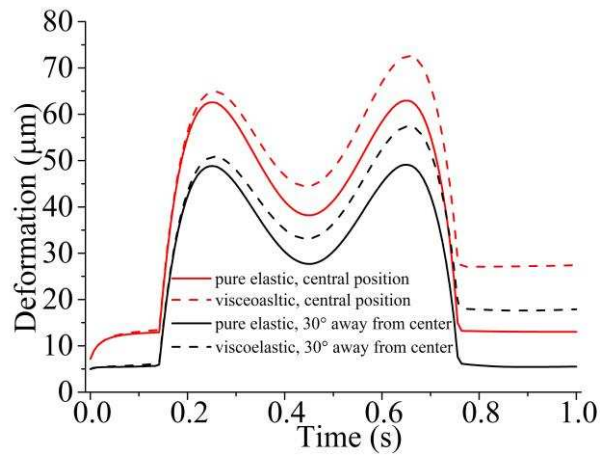
Fig. 7 Elastic and viscoelastic deformations of a node at the center and a node 30° away from center of UHMWPE cup (E_1/E_2=0.14, T=37℃,τ=13.81s)
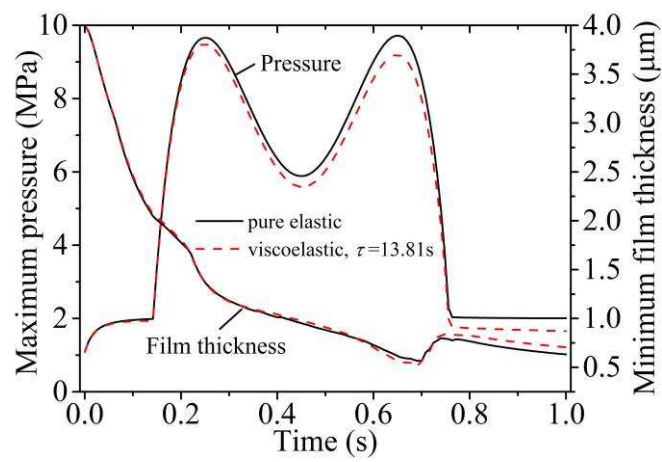
Fig. 8 The comparison of the maximum hydrodynamic pressure and minimum film thickness between the elastic model (E_1/E_2=0.14, T=37°C) and the viscoelastic model during a walking cycle

(a) Pressure   (b) Film thickness
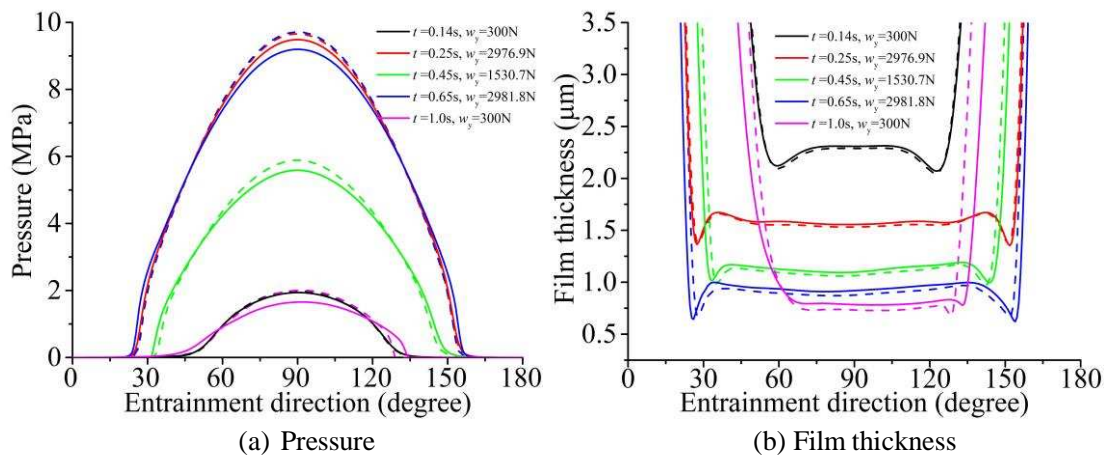
Dash line: elastic model; Solid line: viscoelastic model, relaxation time τ =13.81s

Fig. 9 The variation of the hydrodynamic pressure (a) and film thickness (b) along the entrainment direction with time (E_1/E_2=0.14, T=37℃)
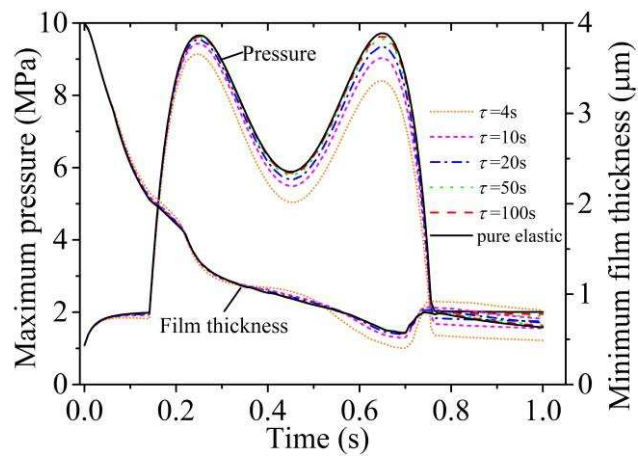
Fig. 10 The variation in the maximum pressure and minimum film thickness of the elastic and viscoelastic models for different relaxation times in a walking cycle

t =0.25s

t =0.45s

t =0.65s

t =1.0s
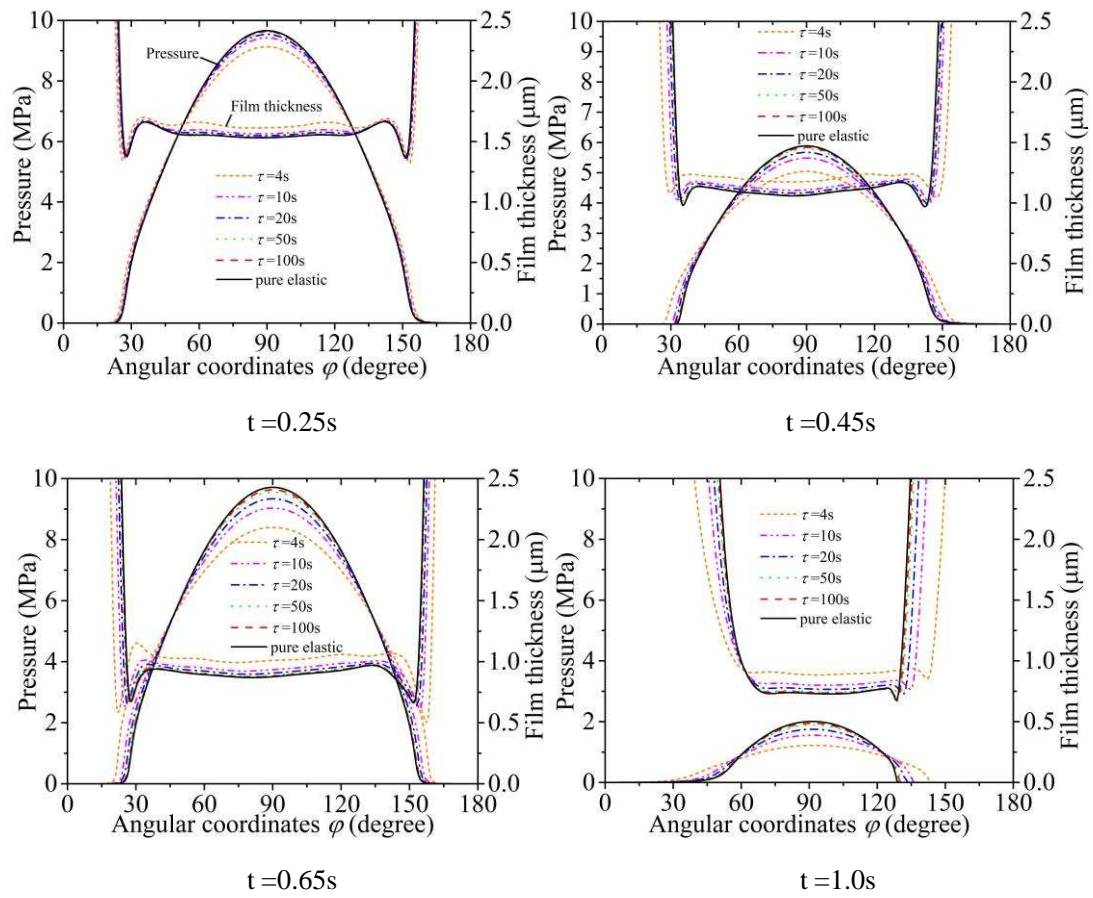
Fig. 11 The comparison of the pressure and film thickness along the entrainment direction between different retardation times and the elastic model at several time instants
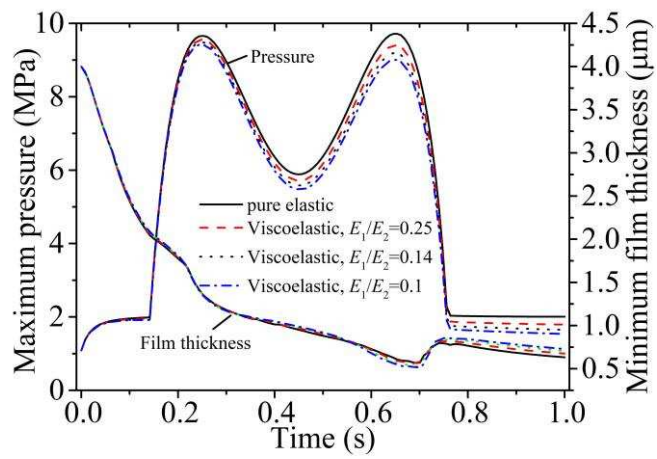
Fig. 12 The comparisons of maximum pressure and minimum film thickness in a walking cycle between different mechanical loss factors (E1/E2)
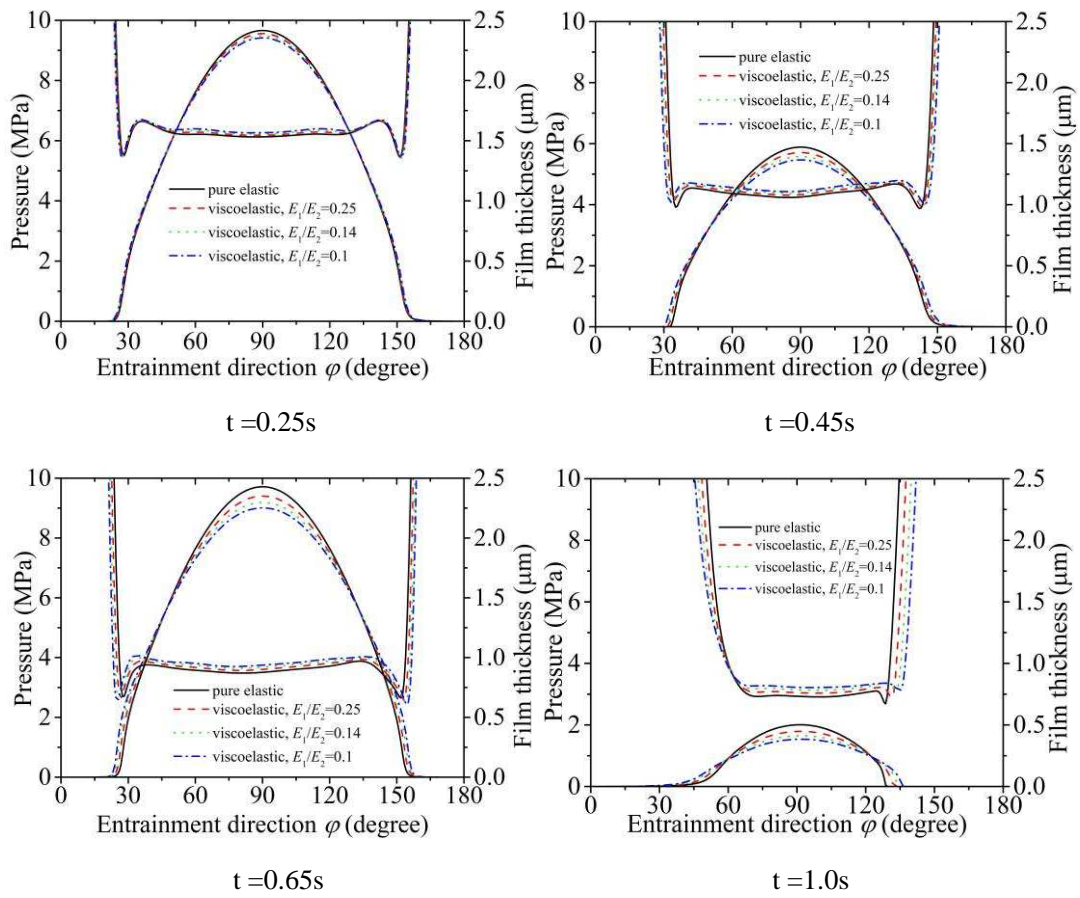
Fig. 13 The pressure and film thickness along the entrainment direction between different mechanical loss factors (E1/E2) and the elastic model at several time instants